



STAR FORMATION

Structural analysis of open cluster Bochum 2

HARMEEN KAUR^{1,*} , SAURABH SHARMA², ALOK DURGAPAL¹,
LOKESH K. DEWANGAN³, AAYUSHI VERMA², NEELAM PANWAR², RAKESH PANDEY³
and ARPAN GHOSH²

¹Center of Advanced Study, Department of Physics, DSB Campus, Kumaun University, Nainital 263002, India.

²Aryabhata Research Institute of Observational Sciences (ARIES), Manora Peak, Nainital 263002, India.

³Physical Research Laboratory, Navrangpura, Ahmedabad 380009, India.

*Corresponding author. E-mail: harmeenkaur.kaur229@gmail.com

MS received 7 February 2023; accepted 30 March 2023

Abstract. We present the results from our deep optical photometric observations of Bochum 2 (Boc2) star cluster obtained using the 1.3-m Devasthal Fast Optical Telescope along with archival photometric data from Pan-STARRS2/2MASS/UKIDSS surveys. We also used high-quality parallax and proper motion data from the Gaia Data Release 3. We found that the Boc2 cluster has a small size (~ 1.1 pc) and circular morphology. Using Gaia parallax of member stars and isochrone fitting method, the distance of this cluster is estimated as 3.8 ± 0.4 kpc. We have found that this cluster holds young (~ 5 Myr) and massive (O7–O9) stars as well as an older population of low mass stars. We found that the massive stars were formed in the inner region of the Boc2 cluster in a recent epoch of star formation. We have derived mass function slope (Γ) in the cluster region as -2.42 ± 0.13 in the mass range of $\sim 0.72 < M/M_{\odot} < 2.8$. The tidal radius of the Boc2 cluster (~ 7 – 9) is much more than its observed radius (~ 1.1 pc). This suggests that most of the low-mass stars in this cluster are the remains of an older population of stars formed via an earlier epoch of star formation.

Keywords. Open star clusters—star formation—massive star—mass function.

1. Introduction

Young open clusters are distinctive to understand the process of star formation and stellar evolution. The young star clusters contain both high-mass and low-mass stars. The physical properties of stars along with the distribution of ionized gas, dust (cold as well as warm) and molecular gas can give us observational hints about the physical processes that conduct their formation and evolution (Jose *et al.* 2008). Many star cluster also show the distribution of massive stars towards their central region. Whether this segregation of massive stars occurs due to an evolutionary effect or is of primordial origin is vague (Lada *et al.* 2006).

For the present study, we have selected Bochum 2 young open cluster, hereafter Boc2, centered at α_{J2000} :

$06^{\text{h}}48^{\text{m}}51.6^{\text{s}}$, δ_{J2000} : $+00^{\circ}23'32.719''$ is shown in Figure 1. This cluster is located in Galactic plane towards the 3rd quadrant ($l = 212^{\circ}.28878$, $b = -0^{\circ}.39462$) in the far northern outskirts of an HII region Sh 2-284. Russeil *et al.* (2007) have proposed that these regions are part of a star forming region located in the Milky Way's Norma (Outer) arm at a distance of 7.9 ± 0.3 kpc. During a search through the catalog of luminous stars, Moffat & Vogt (1975) identified Boc2 cluster that accommodate O-type stars. Moffat *et al.* (1979) provided information about the MK spectral types of the three brightest member stars of the Boc2 cluster as O9V, O7V and O9V. They also spectroscopically derived mean reddening of $E(B - V) = 0.84$ mag and a distance of 4.8 kpc for this cluster. Later, Turbide & Moffat (1993) found differential reddening within the cluster and reported the distance, reddening and age of this cluster as ~ 5.5 kpc, $E(B - V) = 0.89$ mag and 5 Myr, respectively. Munari & Carraro (1995) undertook spectrophotometric studies of this cluster and estimated the distance, mean

This article is part of the Special Issue on “Star formation studies in the context of NIR instruments on 3.6 m DOT”.

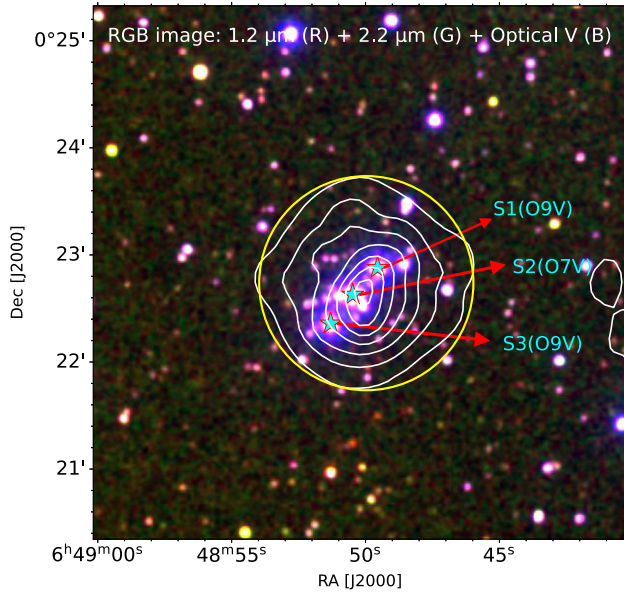


Figure 1. Color-composite image of Boc2 cluster region (red: 2MASS J band ($1.2 \mu\text{m}$); green: 2MASS K band ($2.2 \mu\text{m}$) and blue: Optical V band, taken from 1.3m DFOT) overlaid with the white isodensity contours generated from the NIR catalog (2MASS+UKIDSS; cf. Section 3.1). The lowest level for the isodensity contours is 3σ above the mean stellar density (i.e., $0.29 \text{ stars arcmin}^{-2}$) with a step size of 1σ ($0.1 \text{ stars arcmin}^{-2}$). Yellow circle encloses the lowest density contour, which delineates cluster's region having a radius $1'$. Three massive stars located inside the cluster region are also marked with star symbols along with their spectral type (cf. Section 3.3).

reddening and age of the cluster as $\sim 6 \text{ kpc}$, $E(B - V) = 0.80$ and 7 Myr , respectively. They also confirmed the spectral type of brightest stars, earlier derived by Moffat *et al.* (1979). Recently, Kharchenko *et al.* (2016) studied the Galactic star cluster population based on the Milky Way Star Cluster (MWSC) survey. To determine cluster parameters and membership, they used a combination of uniform kinematic and NIR photometric data gathered from the all-sky catalog PPMXL (Roeser *et al.* 2010). The study estimated distance, extinction and age of this cluster as 2.8 kpc , $E(B - V) = 0.87 \text{ mag}$ and 4.6 Myr .

All the previous studies on Boc2 were based on the shallow optical data and not so precise membership estimation of the cluster members were done. Therefore, with the availability of high quality proper motion data from Gaia DR3 (Gaia Collaboration *et al.* 2016, 2018b) along with new deep and wide-field multi band (optical-to-near-infrared) data sets (cf. Section 2), we have revisited the Boc2 cluster to study in detail about the formation and evolution processes of stars. Also, the extracted parameters of this cluster can be

utilized to enrich the sample of clusters required to study Galactic structure and dynamics.

The structure of this paper is as follows: In Section 2, a brief description of observation and data reduction, and the details of available data sets from various archives is presented. Section 3 describes result and analysis of this study, which includes the study of the structure of this cluster, membership probability and the estimation of basic parameters of the cluster (i.e., extinction, distance, age, mass function, etc.). In Section 4, we discussed about the results and concluded them in Section 5.

2. Observation and data reduction

2.1 Optical data set

The optical CCD $UBVI_c$ photometric data of the Boc2 cluster, centered at $\alpha_{J2000}: 06^{\text{h}}48^{\text{m}}51.6^{\text{s}}$, $\delta_{J2000}: +00^{\circ}23'32.719''$, were acquired by using the $2048 \times 2048 \text{ pixel}^2$ CCD mounted on F/4 cassegrain focus of Devasthal Fast Optical Telescope (DFOT) ARIES, Nainital, India. The entire chip covers a field-of-view (FOV) of $\sim 18.5 \times 18.5 \text{ arcmin}^2$ (plate scale: $0.54 \text{ arcsec per pixel}$). To improve the signal-to-noise ratio (SNR), the observations were carried out in the binning mode of $2 \times 2 \text{ pixels}$. The read-out noise and gain of the CCD are $8.29 e^-$ and $2.2 e^-/\text{ADU}$, respectively. The average FWHM (stellar profile) of the stars were $\sim 2.2 \text{ arcsec}$. The broad-band $UBVI_c$ observations of the Boc2 cluster were standardized by observing stars in the SA98 field (Landolt 1992). A number of bias frames and twilight-flat frames were also taken during observations. Short and deep (long) exposure frames were taken to observe both bright and faint stars in the field. The complete log of the observations is given in Table 1.

The CCD data frames were reduced by using the computing facilities available at the Center of Advanced Study, Department of Physics, Kumaun University, Nainital and ARIES, Nainital. Initial processing of the data frames were done by using the IRAF¹ and ESO-MIDAS² data reduction packages. Photometry of the cleaned frames were carried out by using DAOPHOT-II software (Stetson 1987). The point spread function (PSF) was obtained for each frame by using several uncontaminated stars. We used the DAOGROW

¹IRAF is distributed by National Optical Astronomy Observatories, USA.

²ESO-MIDAS is developed and maintained by the European Southern Observatory.

Table 1. Log of observations.

Date of observations/filter	Exp. (s) × no. of frames
SA98	10 January 2013
<i>U</i>	60 × 1, 90 × 3, 120 × 2
<i>B</i>	30 × 1, 40 × 3, 60 × 2
<i>V</i>	30 × 1, 40 × 5
<i>I_c</i>	10 × 1, 20 × 5
Bochum 2	10 January 2013
<i>U</i>	20 × 3, 600 × 3
<i>B</i>	10 × 3, 600 × 3
<i>V</i>	10 × 3, 600 × 3
<i>I_c</i>	10 × 3, 600 × 4

program for construction of an aperture growth curve required to determine the difference between the aperture and profile-fitting magnitudes. Calibration of the instrumental magnitudes to the standard system was done by using the procedures outlined by Stetson (1992). The total 40 standard stars were used in the photometric calibration of this cluster. The calibration equations derived by the least-squares linear regression are as follows:

$$u = U + (5.380 \pm 0.007) - (0.054 \pm 0.008)(U - B) + (0.433 \pm 0.009)X_U, \quad (1)$$

$$b = B + (4.537 \pm 0.015) - (0.192 \pm 0.011)(B - V) + (0.215 \pm 0.015)X_B, \quad (2)$$

$$v = V + (3.296 \pm 0.009) + (0.009 \pm 0.006)(V - I_c) + (0.101 \pm 0.008)X_V \quad (3)$$

and

$$i_c = I_c + (3.284 \pm 0.005) + (0.000 \pm 0.002) \times (V - I_c) + (0.039 \pm 0.006)X_I, \quad (4)$$

where *U*, *B*, *V* and *I_c* are the standard magnitudes and *u*, *b*, *v* and *i_c* are the instrumental aperture magnitudes, which are normalized per second of exposure time and *X_U*, *X_B*, *X_V* and *X_I* are the airmass in respective filters.

We have also carried out a comparison of the present photometric data with available APASS data. The difference $\Delta(\text{present} - \text{apass})$ as a function of *V* magnitude is shown in Figure 2. The comparison indicates that the magnitudes obtained in the present work are in fair agreement with those available in the literature. The distinctive DAOPHOT errors in different bands as a function of *V* magnitude shown in Figure 3. In this, bright and faint stars are taken from short and long frames, respectively. It can be seen that at fainter magnitude, limit errors become large (>0.1) and were

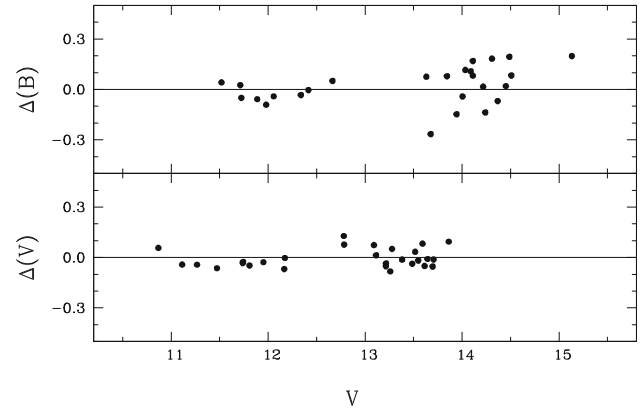


Figure 2. Comparison of present photometric data with available apass data as a function of present *V* magnitude.

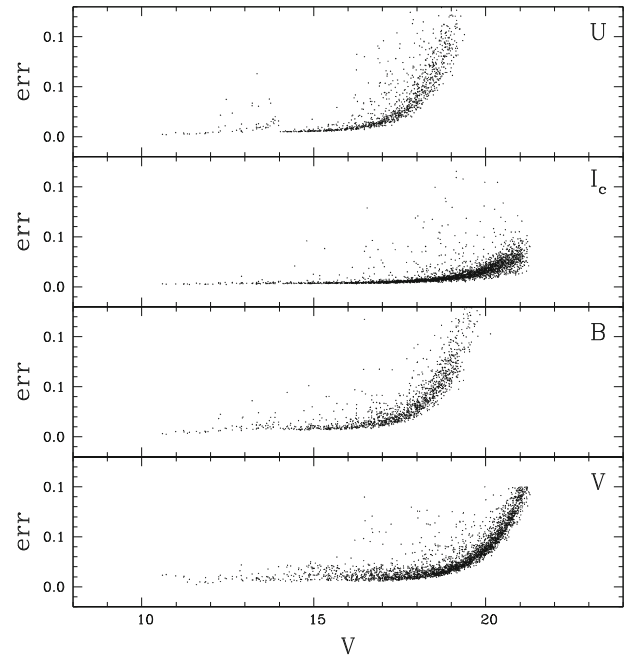


Figure 3. *V*, *B*, *I_c*, *U* photometric errors as a function of *V* magnitude.

not used in the present work. In this study, a total of 2824 sources have been identified with detection at least in the *V* and *I_c* bands and having photometric errors <0.1 mag up to *V* ~ 21.3 mag.

2.2 Archival data sets

We used the near-infrared (NIR) point source catalog³ and images⁴ from 2MASS (Cutri *et al.* 2003;

³<https://irsa.ipac.caltech.edu/Missions>.

⁴<https://skyview.gsfc.nasa.gov/current/cgi/query.pl>.

Skrutskie *et al.* 2006) and UKIDSS⁵ (Lawrence *et al.* 2007). We have also used the Panoramic Survey Telescope and Rapid Response System⁶ (PanSTARRS1 or PS1) data release 2 (Chambers *et al.* 2016) and recently available high quality proper motion data from Gaia⁷ Data Release 3 (Gaia Collaboration *et al.* 2018a). For our photometric analysis, we used only those sources which have uncertainties <0.1 mag.

3. Results and analysis

3.1 Structure of Boc 2 cluster

As literature put forwards, this cluster is young and have distribution of gas and dust around it. We have used the stellar number density profile, obtained from the NIR catalog of stars, to study the structure of this cluster (cf. Figure 1). The NIR catalog is compiled from the 2MASS (for stars with $J_{\text{mag}} < 13$; bright stars) and UKIDSS (for stars with $J_{\text{mag}} \geq 13$; faint stars) surveys covering $18'.5 \times 18'.5$ FOV (similar to our optical observations) around the cluster region. The stellar number density maps were generated using the nearest neighbor (NN) method as described by Gutermuth *et al.* (2005) and Sharma *et al.* (2020). We took the radial distance necessary to encompass the 20th nearest stars and computed the local surface density in a grid size of 6 arcsec (Gutermuth *et al.* 2009). Figure 1 constitutes the color image of $5' \times 5'$ area around the Boc2 cluster region, composed with red: 2MASS J band ($1.2 \mu\text{m}$); green: 2MASS K band ($2.2 \mu\text{m}$) and blue: Optical V band, taken from 1.3m DFOT. The stellar number density contours derived by above method are superimposed in Figure 1 as white contours smoothed to a grid of size 3×3 pixels. The lowest contour is 3σ above the mean of stellar density ($0.29 \text{ star arcmin}^{-2}$) with a step size of 1σ ($0.1 \text{ stars arcmin}^{-2}$). Although the bright stars in the cluster region suggest an elongated morphology, whereas the cluster obtained from deep NIR isodensity contours show almost circular morphology. The yellow circle in Figure 1 encloses the lowest density contour and delineates cluster region with a radius of 1 arcmin centered at $\alpha_{J2000}: 06^{\text{h}}48^{\text{m}}50.17^{\text{s}}$, $\delta_{J2000}: +00^{\circ}22'42.17''$. Inside the cluster region (lowest density contour or yellow circle of radius $1'$), three massive stars are also marked as star symbols in Figure 1. These stars are named as S1, S2 and S3 with spectral type O9V,

O7V and O9V, respectively (for details, refer Munari & Carraro 1995).

3.2 Membership probability

The astrometric selection of the cluster's members in large scale was always limited by the errors of the proper motions given by the catalogs before the Gaia mission. Better membership determination made possible by the new generation of high precision astrometric Gaia DR3 catalog up to very faint limits⁸ (Gaia Collaboration *et al.* 2016, 2018b). To determine the membership probability using Gaia DR3, we adopted the method described in Balaguer-Núñez *et al.* (1998). This method is efficiently used before in many studies (Kaur *et al.* 2020; Pandey *et al.* 2020; Sharma *et al.* 2020). In this method, we first construct the frequency distributions of cluster stars (ϕ_c^v) and field stars (ϕ_f^v) using the following equations given in Yadav *et al.* (2013). The Gaia proper motion (PM) data of the stars located within the Boc2 cluster region is used to determine their membership probability. The PMs, $\mu_\alpha \cos(\delta)$ and μ_δ are plotted as vector-point diagrams (VPDs) in the panel 1 of Figure 4. The panel 2 shows the corresponding G vs. $G_{\text{BP}} - G_{\text{RP}}$ Gaia color-magnitude diagrams (CMDs). The tight clump centering at $\mu_{xc} = -0.175 \text{ mas yr}^{-1}$, $\mu_{yc} = 0.133 \text{ mas yr}^{-1}$, having radius of 0.8 mas yr^{-1} in the VPD represents the probable cluster stars, and the remaining represents the distribution of the probable field stars. The left sub-panels show all stars, while the middle and right sub-panels show the probable cluster members and field stars. Assuming a distance of 3.8 kpc (estimated in present study cf. Section 3.3) and a radial velocity dispersion of 1 km s^{-1} for open clusters (Girard *et al.* 1989), the expected dispersion (σ_c) in PMs of the cluster would be $\sim 0.05 \text{ mas yr}^{-1}$. From the distribution of probable field stars, we have calculated $\mu_{xf} = -0.26 \text{ mas yr}^{-1}$, $\mu_{yf} = -0.55 \text{ mas yr}^{-1}$, $\sigma_{xf} = 1.90 \text{ mas yr}^{-1}$ and $\sigma_{yf} = 1.90 \text{ mas yr}^{-1}$. These values are further used to construct the frequency distribution of cluster stars (ϕ_c^v) and field stars (ϕ_f^v) by using the equations given in Yadav *et al.* (2013) and then, the value of membership probability of the cluster is estimated by using the following equation:

$$P_\mu(i) = \frac{n_c \times \phi_c^v(i)}{n_c \times \phi_c^v(i) + n_f \times \phi_f^v(i)}, \quad (5)$$

where n_c ($=0.48$) and n_f ($=0.52$) are the normalized numbers of stars for the cluster and field region ($n_c + n_f = 1$). The membership probability (estimated

⁵<http://wsa.roe.ac.uk>.

⁶<https://catalogs.mast.stsci.edu/>.

⁷<https://gea.esac.esa.int/archive/>.

⁸<https://gea.esac.esa.int/archive/>.

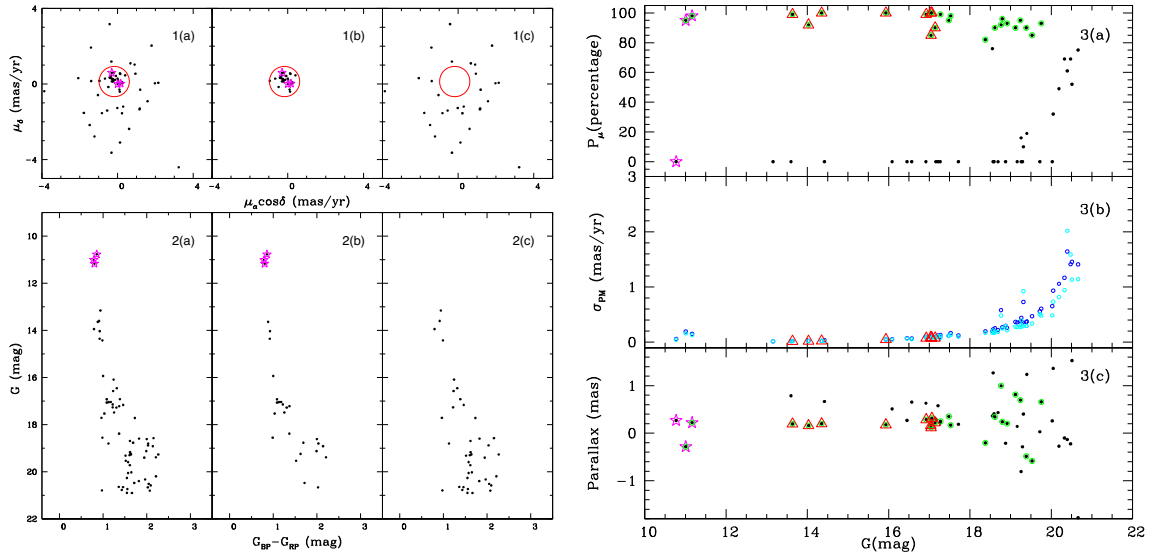


Figure 4. Panel 1 shows the PM vector-point diagrams (VPDs) and panel 2 shows G_{mag} vs. $G_{\text{BP}} - G_{\text{RP}}$ CMDs. The left sub-panels (1(a) and 2(a)) show all stars located within Boc2 cluster region (cf. Section 3.1), while the middle (1(b) and 2(b)) and right sub-panels (1(c) and 2(c)) show the probable cluster members and field stars. Panel 3 depicts the membership probability (P_μ), PM errors (σ_{PM}) and parallax of stars in the cluster region as a function of G magnitude. The probable member stars ($P_\mu > 80$) are shown by green circles, while the nine members used for distance estimation of the Boc2 cluster are depicted by red triangles (see text for details). Location of massive stars (O-type) can also be seen in all panels by star symbols.

above), errors in the PM and parallax values are plotted as a function of G magnitude in panel 3 of Figure 4. As can be seen in these plots, a high membership probability ($P_\mu > 80\%$) extends down to $G \sim 20$ mag. At brighter magnitudes, there is a clear separation between cluster members and field stars that reinforce this technique. Errors in PMs become very high at faint limits, and the maximum probability gradually decreases at those levels. Therefore, on the basis of above analysis, 24 stars were assigned as cluster members of Boc2 cluster based on their high membership probability $P_\mu > 80\%$ (green circles with black rings in Figure 4). Location of massive stars (O-type; cf. Section 3.1) are also shown in all panels by the magenta star symbol.

3.3 Reddening, distance and age of the cluster

The reddening in the direction of a cluster can be derived quite accurately by using the two-color diagrams (TCDs) (cf., Phelps & Janes 1994; Sharma *et al.* 2006). In the left panel of Figure 5, we show the $(U - B)$ vs. $(B - V)$ TCD of the stars located inside the Boc2 cluster. The identified member stars (green circles) from the Gaia data and most massive stars (magenta star symbols) located inside the cluster region are also marked in the figure. To estimate the reddening in the cluster direction, the intrinsic zero-age main sequence (ZAMS, Pecaut & Mamajek 2013, for $Z = 0.02$) is shifted along

the reddening vector ($E(B - V)/E(U - B) = 0.72$), so that it matches with the distribution of member stars. The amount of shift in the X-axis gives a reddening, $E(B - V)$, value of the cluster. The blue continuous curve and red dotted curve are the ZAMS, which are visually fitted to estimate the reddening value for the foreground stars ($E(B - V)_f = 0.45$ mag) and the massive stars ($E(B - V)_{cl} = 0.80$ mag), respectively. As the massive stars are members of the Boc2 cluster, we designated their reddening as cluster reddening value.

As already discussed in Section 1, there is a large discrepancy in the earlier reported values of the distance of Boc2 cluster, i.e., 2.8–6 kpc. We have used the Gaia data to revise the distance estimate of this cluster. For this purpose, we have selected nine cluster members having parallax error < 0.1 (red triangles in Figure 4) and calculated the mean of the photo-geometric distances as reported by Bailer-Jones *et al.* (2021). Thus, the distance of Boc2 cluster comes out to be $\sim 3.8 \pm 0.4$ kpc. We further cross checked this estimated distance by using the color–magnitude diagrams (CMDs) (Phelps & Janes 1994; Pandey *et al.* 2020, 2022; Sharma *et al.* 2020). In the right panel of Figure 5, we have shown the V vs. $(V - I)$ CMD for the stars in the cluster region. The member and massive stars are also marked in the figure. The curves represent the ZAMS from Pastorelli *et al.* (2019) corrected for a distance of 3.8 kpc, and

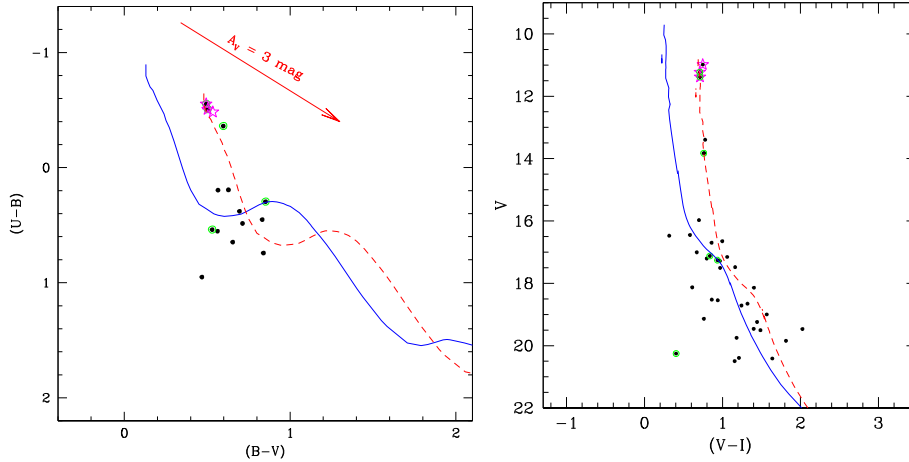


Figure 5. Left panel: $(U - B)$ vs. $(B - V)$ TCD for optically detected sources in the Boc2 cluster region. The blue curve describes the intrinsic Zero Age Main Sequence (ZAMS) for $Z = 0.02$ by Pecaut & Mamajek (2013) shifted along the reddening vector for $E(B - V) = 0.45$ mag. The dotted red curve indicates same ZAMS, but for $E(B - V) = 0.80$ mag. Green open circles and magenta star symbols are the location of cluster members and massive O-type stars, respectively. Right panel: V vs. $(V - I_c)$ CMD for the same sources as described in the left panel. The curves show the ZAMS from Pastorelli et al. (2019) corrected for a distance of 3.8 kpc and reddening $E(B - V) = 0.45$ mag (blue curve) and $E(B - V) = 0.80$ mag (red dotted curve), respectively, for the foreground and cluster reddening values, respectively.

reddening $E(B - V) \sim 0.45$ mag (blue curve) and $E(B - V) \sim 0.80$ mag (red dotted curve), for the foreground and cluster reddening values, respectively. Clearly, the massive stars are falling correctly on the respective massive end of the ZAMS for a distance of 3.8 kpc and $E(B - V) = 0.80$ mag. We have also used PanSTARR1 optical data to substantiate our parameters. For this purpose, we have plotted the g vs. $(g - i)$ CMD for the stars located inside the cluster region (black dots), massive stars (star symbols) and the identified cluster members (green circles) in Figure 6. In left panel of Figure 6, the ZAMS (Pastorelli et al. 2019) corrected for different extinction and distance values (as reported in literature) are shown and in the right panel, the present estimates are used. Certainly, out of different distance and reddening estimates, the ZAMS corrected for the present estimates (distance ~ 3.8 kpc and $E(B - V) \sim 0.80$ mag) seems to be the best match to the distribution of stars within the Boc2 cluster.

As already discussed, the previous studies suggests that this cluster is young (from 4.6 to 7 Myr) in nature (Moffat et al. 1979; Turbide & Moffat 1993; Munari & Carraro 1995; Camargo et al. 2015; Kharchenko et al. 2016). Most of these estimated ages were based on the MS lifetime of the most of the massive stars in the cluster. In Figure 7, we show the J vs. $(J - H)$ CMD for (a) stars within cluster region, (b) stars within reference region (or field region) of same area as of cluster and (c) statistically cleaned sample of stars (see also Sharma et al. 2007, 2012, 2017; Pandey et al. 2008,

2013; Chauhan et al. 2011; Jose et al. 2013). We have also marked the location of massive stars in the CMDs. The clusters CMD distribution matches well with the ZAMS, specially in the lower part of the CMD. Even after the statistical subtraction, the distribution of stars in the lower part of the CMDs stays similar. We have plotted the isochrone of 5 Myr (approximate age of massive stars) over the statistically cleaned CMD. The upper end of the CMD (location of massive stars) is matching well with the 5 Myr isochrone, but in the lower-part of the CMD, there are not many stars falling on the 5 Myr isochrone. This kind of distribution suggests an extended history of star formation in this cluster, i.e., the star formation in Boc2 cluster might have started much earlier than the formation of massive stars (cf. Pandey et al. 2005). From the current distribution of stars in the CMDs, its very difficult to constrain the first epoch of star formation in the Boc2 cluster, but the most recent star formation has occurred at 5 Myr ago with the formation of massive stars.

3.4 Mass function

The initial mass function (IMF) is known as the distribution of stellar masses that form in one star formation event in a given volume of space. It is one of the important statistical method to study star formation. Open clusters possess many favorable characteristics for MF studies, e.g., clusters containing almost the coeval set

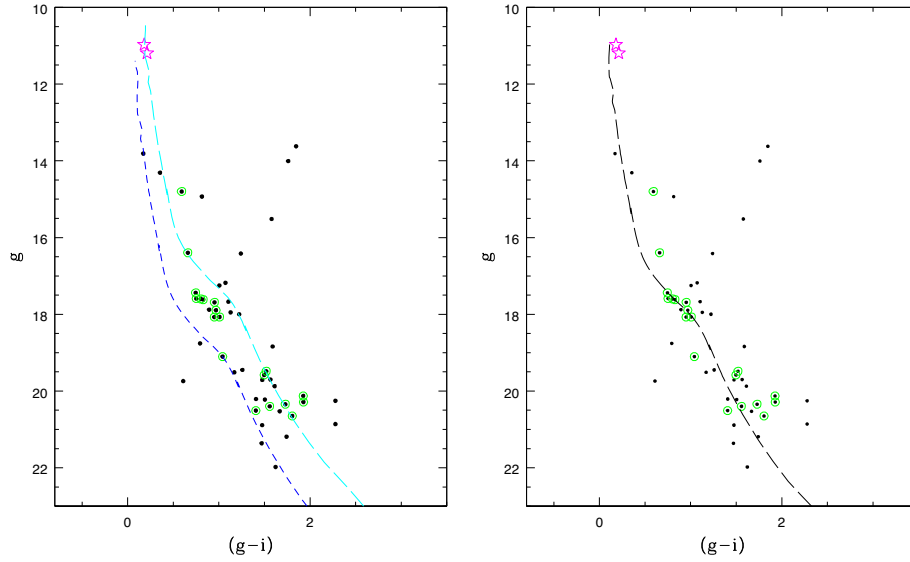


Figure 6. Left panel: PS1 g vs. $(g - i)$ CMD for the stars in the cluster region (black dots). Green open circles and magenta star symbols are the locations of cluster members and massive O-type stars, respectively. The curves denote the ZAMS derived from Pastorelli *et al.* (2019) corrected for extinction and distance values reported in literature, i.e., $A_V = 2.76$ mag, distance = 5.5 kpc (blue dashed curve) (Moffat & Vogt 1975) and $A_V = 2.70$ mag, distance = 2.8 kpc (cyan dashed curve) (Kharchenko *et al.* 2016). Right panel: Same as left panel, but with ZAMS corrected for a distance of 3.8 kpc and reddening of $E(B - V) = 0.80$ mag (present work, black dashed curve).

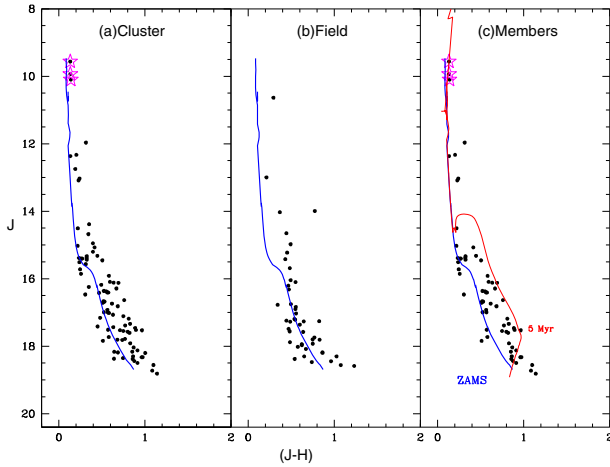


Figure 7. J vs. $(J - H)$ CMD for (a) stars within the cluster region, (b) stars within the reference field of same area as of the cluster and (c) statistically cleaned sample, which is over-plotted with the ZAMS (solid blue curve) and the 5 Myr isochrone (solid red curve) taken from Pastorelli *et al.* (2019). All the isochrones have been corrected for a distance of 3.8 kpc and reddening $E(B - V) = 0.80$ mag. Location of massive stars are shown by the magenta star symbols.

of stars at the same distance with the same metallicity; hence, difficulties such as complex corrections for stellar birth rates, life times, etc., associated with determining the MF from field stars are automatically removed. The MF is often expressed by a power law,

$N(\log m) \propto m^\Gamma$, and the slope of the MF is given as:

$$\Gamma = \frac{d(\log m)}{d \log m}, \quad (6)$$

where $N \log(m)$ is the number of stars per unit logarithmic mass interval. The luminosity function (LF) of the cluster is converted into MF using a theoretical evolutionary track (Pecaut & Mamajek 2013). To obtain the LF, we generate J vs. $(J - H)$ CMD from the NIR data (cf. Figure 8), corrected for the data incompleteness, distance and extinction (see Sharma *et al.* 2020). In Figure 8, we show the CMD for the cluster region as well as for the field region (α_{J2000} : $06^{\text{h}}49^{\text{m}}08.67^{\text{s}}$, δ_{J2000} : $+00^{\circ}27'32.36''$), having the same area. The contamination due to field stars is greatly reduced by selecting a sample of stars which are located near the well-defined main sequence (MS) (cf. Sharma *et al.* 2008, 2020). Thus, we have generated an envelope of $+0.3$ mag and -0.2 mag around the CMD considering the distribution of member stars and is shown in the left panel of Figure 8. The number of probable cluster members were obtained by subtracting the contribution of field stars (corrected for data incompleteness), in different magnitude bins, from the contaminated sample of cluster stars (corrected for data incompleteness).

The photometric data can be incomplete due to various reasons, e.g., nebulosity, crowding of the stars, detection limit, etc. We estimated the completeness of NIR data by using the distribution of star number

in different mag bins as shown in the left panel of Figure 9. The peak in the stellar number distribution will more or less represent the complete sample after which the completeness of the photometric data tends to decrease (see also, Jose *et al.* 2017; Sharma *et al.* 2020). Thus, we have found that the present NIR data (2MASS+UKIDSS) is complete up to ~ 17.5 mag in J band, corresponding to a star of $\sim 0.9 M_{\odot}$ at a distance

of 3.8 kpc. For the stars in mag bin 17.5–18.5 in J band, we have used the completeness factor of 80% (see also, Jose *et al.* 2017; Sharma *et al.* 2020). The resultant MF distribution in the cluster region is shown in the right panel of Figure 9.

4. Discussion

It is known that the higher mass stars mostly follow the Salpeter MF ($\Gamma = -1.35$; Salpeter 1955). At lower masses, the MF is less constrained, but appears to flatten below $1 M_{\odot}$ and exhibits few stars of the lowest masses (Kroupa & Boily 2002; Chabrier 2003; Luhman *et al.* 2016). In this study, we found that the MF distribution in the lower mass bins ($\sim 0.72 < M/M_{\odot} < 2.8$) is showing a well-defined linear distribution (cf. left panel of Figure 9), and has a slope (-2.42 ± 0.13), which is very much steeper than the Salpeter value (-1.35). This indicates toward the presence of the excess number of low mass stars in the Boc2 cluster. This apparent excess of low mass stars could be due to the stellar evolutionary effects in which massive stars could have evolved off from the MS. If we consider massive stars in the distribution ($\sim 0.72 < M/M_{\odot} < 19.6$), the value Γ becomes shallow (-0.95 ± 0.24 , cf. left panel of Figure 9), indicating the formation of massive stars in the recent epoch of star formation. The age analysis in Section 3.3 also suggest similar results in which low mass stars in the Boc2 cluster which might have formed at an earlier epoch of star formation than the massive ones.

To investigate further, we have calculated the mass segregation ratio (MSR) as a measure to quantify mass segregation in the cluster region by using Allison *et al.* (2009) method. In this approach, we constructed the minimum sampling tree (MST) for the massive stars

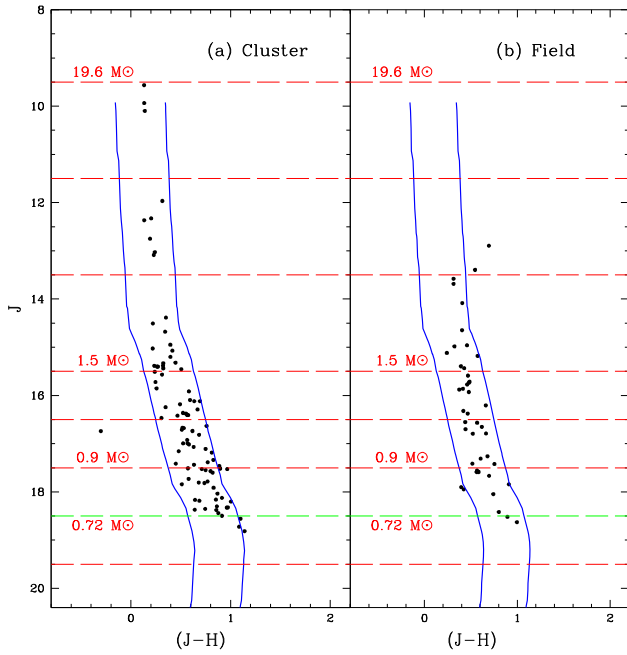


Figure 8. J vs. $(J-H)$ CMD for (a) stars within the cluster region and (b) stars within the field or reference region of the same area as of cluster. The curves denotes envelop of $+0.3$ mag (right curve; $A_v = 2.42$ mag) and -0.2 mag (left curve; $A_v = 1.88$ mag) around the CMD from the isochrone of Pecaut & Mamajek (2013). Green horizontal line shows the magnitude limit corresponding to the completeness factor of 80%.

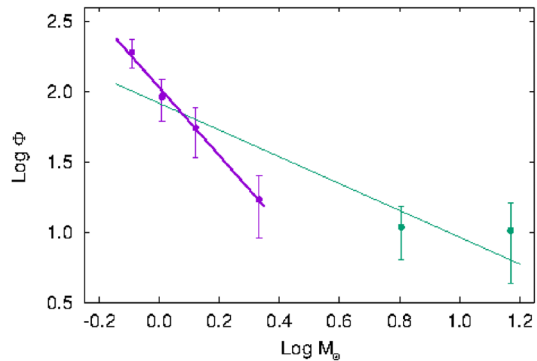
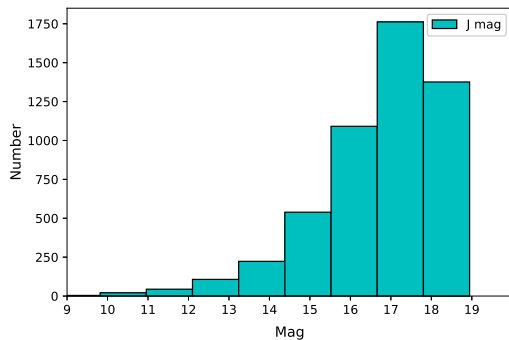


Figure 9. Left panel: Histogram shows the data completeness of J mag of NIR data. Right panel: A plot of the mass function (MF) for the Boc2 cluster using NIR data. $\text{Log } \phi$ represent $\log(N/d \log m)$ and the error bars represent standard $\pm \sqrt{N}$ errors. The solid line shows a least squares fit to the MF distribution.

and for the equal number of randomly selected stars from the cluster sample and estimated their mean edge length as γ^{mp} and γ^{rand} , respectively. Therefore, the value of Γ_{MSR} (cf. [Olczak et al. 2011](#); [Dib et al. 2018](#); [Sharma et al. 2020](#)) is estimated as:

$$\Gamma_{MSR} = \frac{\langle \gamma_{MST}^{rand} \rangle}{\gamma_{MST}^{mp}}. \quad (7)$$

A value of $\Gamma_{MSR} \sim 1$ implies that both most massive and randomly selected samples of stars are distributed in a similar manner, whereas $\Gamma_{MSR} > 1$ indicates mass segregation and $\Gamma_{MSR} \ll 1$ points to inverse mass segregation ([Dib et al. 2018](#)). To minimize the uncertainties associated with the conversion of luminosity to mass, we have used magnitude of cluster stars (cf. [Figure 8](#)) as a proxy to their masses (cf. [Dib et al. 2018](#)). For the Boc2 cluster, we derived $\Gamma_{MSR} = 1.3 \pm 0.9$, which suggests the effect of mass segregation in this cluster. To further check, whether mass segregation is primordial or due to dynamical relaxation, we estimated the dynamical relaxation time, T_E , the time in which the individual stars exchange sufficient energy so that their velocity distribution approaches that of a Maxwellian equilibrium using the method given by [Binney & Tremaine \(1987\)](#):

$$T_E = \frac{N}{8} \times T_{cross}, \quad (8)$$

where $T_{cross} = D/\sigma_v$ denotes the crossing time, N is the total number of stars in the cluster region under study of diameter D , and σ_v is the velocity dispersion, with a typical value of 3 km s^{-1} ([Bisht et al. 2017](#)). For the Boc2 cluster, the value of dynamical relaxation time is $T_E \sim 8 \text{ Myr}$ (cf. [Sharma et al. 2020](#)). If we assume the loss of 50% of stars due to incompleteness of our data, the dynamical relaxation time will be $T_E \sim 14 \text{ Myr}$, which is more than the age of the massive stars in the Boc2 cluster (i.e., $\sim 5 \text{ Myr}$). This suggest that massive stars in the Boc2 cluster have formed in the inner regions of this cluster.

As the cluster becomes older, the stars escape from the cluster region because of various processes. These can be divided into internal and external processes. Internal processes are like two body relaxation and dynamical relaxation ([Dalessandro et al. 2015](#)), and external processes are like tidal interaction and encounters with molecular clouds, spiral arm and Galactic disc ([Gieles et al. 2006](#); [Gieles & Baumgardt 2008](#); [Yeh et al. 2020](#)). Since, the Boc2 cluster hosts older generation of low mass stars, there is also a possibility that some of them escaping from the cluster region. Thus, we have calculated the tidal radius of this star cluster by using

the equation given by [Pinfield et al. \(1998\)](#):

$$r_t = \left[\frac{GM_C}{2(A - B)^2} \right]^{1/3}, \quad (9)$$

where G is the gravitational constant, M_C is the total mass of the cluster, and A and B are the Oort constants, $A = 15.3 \pm 0.4 \text{ km s}^{-1} \text{ kpc}^{-1}$, $B = -11.9 \pm 0.4 \text{ km s}^{-1} \text{ kpc}^{-1}$ ([Bovy 2017](#)). From the conversion of LF into MF (cf. [Section 3.4](#)), mass of the Boc2 cluster is estimated as $M_C = 126 M_\odot$. The corresponding tidal radius appears to be $\sim 7 \text{ pc}$. This is a good approximation even if we have missed 50% of the cluster mass in the lower mass bins due to data incompleteness, then the resultant tidal radius will be $\sim 9 \text{ pc}$. Therefore, we can conclude that the tidal radius ($r_t \sim 7 \text{ pc}$) of this cluster is much larger than the present estimate of the cluster radius ($R_{cluster} \sim 1.1 \text{ pc}$). Hence, the observed small size of this cluster resembles a remains of an old population of stars formed via a earlier epoch of star formation. A recent epoch of the star formation activity in this cluster might be responsible for the formation of massive stars in this cluster. The formation of a new generation of stars in this cluster might be explained by the process given in [Pflamm-Altenburg & Kroupa \(2009\)](#), suggests if the open cluster moves through a molecular cloud, it will accrete gas recurrently from the surrounding medium which may source further star formation events and account for multiple stellar populations in the cluster.

5. Summary and conclusion

We have performed a deep ($V \sim 21.3 \text{ mag}$) and wide-field (FOV $\sim 18.5 \times 18.5 \text{ arcmin}^2$) multiband (UBVI_c) photometric observations around the Boc2 cluster. The optical data along with Gaia DR3 and deep PanSTARR1 (PS2) data have been used to study the membership probability of stars in the cluster region, structural parameters of the cluster, MF and mass segregation in the Boc2 cluster. The main results are summarized as follows:

- We have derived the structural parameters of the Boc2 cluster by using isodensity contour (NN method) analysis and found that this cluster shows circular morphology. The cluster is having radius of 1 arcmin (1.1 pc) and is centered at $\alpha_{J2000}: 06^{\text{h}}48^{\text{m}}50^{\text{s}}$, $\delta_{J2000}: +00^{\circ}22'43.611''$.
- Using Gaia DR3 proper motion data, we have identified 24 stars as most probable cluster members of the cluster Boc2. The distance of this

cluster, as estimated from the Gaia parallax and isochrone fitting method, is $\sim 3.8 \pm 0.4$ kpc. The reddening towards the cluster is estimated as $E(B - V) \sim 0.8$ mag. We also estimated age of the massive candidates of this cluster as ~ 5 Myr. This cluster also seems to hold an older population of low mass stars.

- By using deep NIR data, we also derived MF slope (Γ) in the cluster region as -2.42 ± 0.13 in the mass range of $\sim 0.72 < M/M_{\odot} < 2.8$. This slope is steeper than Salpeter value (-1.35). This indicates the presence of an excess number of low-mass stars in the cluster.
- This cluster shows the effect of mass segregation, whereas the dynamical age (~ 8 – 14 Myr) of this cluster is found to be more than the age of massive stars (~ 5 Myr). This indicates that the massive stars have formed in the inner region of the Boc2 cluster, in a recent epoch of star formation.
- The tidal radius of the Boc2 cluster (~ 7 – 9) is much more than its observed radius (~ 1.1 pc). This indicates that the most of the stars in this cluster are the remnants of an older population of stars formed via an earlier epoch of star formation.

Acknowledgements

The observations reported in this paper were obtained using the 1.3m Devesthal Fast Optical Telescope, Nainital, India. This work is based on data obtained as part of the UKIRT Infrared Deep Sky Survey (UKIDSS). This publication made use of data products from 2MASS (a joint project of the University of Massachusetts and the Infrared Processing and Analysis Center/California Institute of Technology, funded by NASA and NSF) and archival data obtained with the Spitzer Space Telescope (operated by the Jet Propulsion Laboratory, California Institute of Technology, under a contract with NASA). This study has made use of data from the European Space Agency (ESA) mission Gaia (<https://cosmos.esa.int/gaia>), processed by the Gaia Data Processing and Analysis Consortium (DPAC; <https://cosmos.esa.int/web/gaia/dpac/consortium>). Funding for the DPAC has been provided by the institutions participating in the Gaia Multilateral Agreement.

References

- Allison R. J., Goodwin S. P., Parker R. J. *et al.* 2009, MNRAS, 395, 1449
- Bailer-Jones C. A. L., Rybizki J., Fouesneau M., Demleitner M., Andrae R. 2021, AJ, 161, 147
- Balaguer-Núñez L., Tian K. P., Zhao J. L. 1998, A&AS, 133, 387
- Binney J., Tremaine S. 1987, Galactic dynamics
- Bisht D., Yadav R. K. S., Durgapal A. K. 2017, New A, 52, 55
- Bovy J. 2017, MNRAS, 468, L63
- Camargo D., Bonatto C., Bica E. 2015, MNRAS, 450, 4150
- Chabrier G. 2003, PASP, 115, 763
- Chambers K. C., Magnier E. A., Metcalfe N. *et al.* 2016, arXiv e-prints, 1612.05560
- Chauhan N., Pandey A. K., Ogura K. *et al.* 2011, MNRAS, 415, 1202
- Cutri R. M., Skrutskie M. F., van Dyk S. *et al.* 2003, VizieR Online Data Catalog, II/246
- Dalessandro E., Ferraro F. R., Massari D. *et al.* 2015, ApJ, 810, 40
- Dib S., Schmeja S., Parker R. J. 2018, MNRAS, 473, 849
- Gaia Collaboration, Prusti T., de Bruijne J. H. J. *et al.* 2016, A&A, 595, A1
- Gaia Collaboration, Katz D., Antoja T. *et al.* 2018a, A&A, 616, A11
- Gaia Collaboration, Brown A. G. A., Vallenari A. *et al.* 2018b, A&A, 616, A1
- Gieles M., Baumgardt H. 2008, MNRAS, 389, L28
- Gieles M., Portegies Zwart S. F., Baumgardt H. *et al.* 2006, MNRAS, 371, 793
- Girard T. M., Grundy W. M., Lopez C. E., van Altena W. F. 1989, AJ, 98, 227
- Gutermuth R. A., Megeath S. T., Myers P. C. *et al.* 2009, ApJS, 184, 18
- Gutermuth R. A., Megeath S. T., Pipher J. L. *et al.* 2005, ApJ, 632, 397
- Jose J., Herczeg G. J., Samal M. R., Fang Q., Panwar N. 2017, ApJ, 836, 98
- Jose J., Pandey A. K., Ojha D. K. *et al.* 2008, MNRAS, 384, 1675
- Jose J., Pandey A. K., Samal M. R. *et al.* 2013, MNRAS, 432, 3445
- Kaur H., Sharma S., Dewangan L. K. *et al.* 2020, ApJ, 896, 29
- Kharchenko N. V., Piskunov A. E., Schilbach E., Röser S., Scholz R. D. 2016, A&A, 585, A101
- Kroupa P., Boily C. M. 2002, MNRAS, 336, 1188
- Lada C. J., Muench A. A., Luhman K. L. *et al.* 2006, AJ, 131, 1574
- Landolt A. U. 1992, AJ, 104, 340
- Lawrence A., Warren S. J., Almaini O. *et al.* 2007, MNRAS, 379, 1599
- Luhman K. L., Esplin T. L., Loutrel N. P. 2016, ApJ, 827, 52
- Moffat A. F. J., Fitzgerald M. P., Jackson P. D. 1979, A&AS, 38, 197
- Moffat A. F. J., Vogt N. 1975, A&AS, 20, 85
- Munari U., Carraro G. 1995, MNRAS, 277, 1269

- Olczak C., Spurzem R., Henning T. 2011, *A&A*, 532, A119
- Pandey A. K., Sharma S., Ogura K. *et al.* 2008, *MNRAS*, 383, 1241
- Pandey A. K., Upadhyay K., Ogura K. *et al.* 2005, *MNRAS*, 358, 1290
- Pandey A. K., Eswaraiiah C., Sharma S. *et al.* 2013, *ApJ*, 764, 172
- Pandey R., Sharma S., Panwar N. *et al.* 2020, *ApJ*, 891, 8
- Pandey R., Sharma S., Dewangan L. K. *et al.* 2022, *ApJ*, 926, 25
- Pastorelli G., Marigo P., Girardi L. *et al.* 2019, *MNRAS*, 485, 5666
- Pecaut M. J., Mamajek E. E. 2013, *ApJS*, 208, 9
- Pflamm-Altenburg J., Kroupa P. 2009, *MNRAS*, 397, 488
- Phelps R. L., Janes K. A. 1994, *ApJS*, 90, 31
- Pinfield D. J., Jameson R. F., Hodgkin S. T. 1998, *MNRAS*, 299, 955
- Roeser S., Demleitner M., Schilbach E. 2010, *AJ*, 139, 2440
- Russeil D., Adami C., Georgelin Y. M. 2007, *A&A*, 470, 161
- Salpeter E. E. 1955, *ApJ*, 121, 161
- Sharma S., Pandey A. K., Ogura K. *et al.* 2006, *AJ*, 132, 1669
- Sharma S., Pandey A. K., Ogura K. *et al.* 2008, *AJ*, 135, 1934
- Sharma S., Pandey A. K., Ojha D. K. *et al.* 2007, *MNRAS*, 380, 1141
- Sharma S., Pandey A. K., Ojha D. K. *et al.* 2017, *MNRAS*, 467, 2943
- Sharma S., Pandey A. K., Pandey J. C. *et al.* 2012, *PASJ*, 64, 107
- Sharma S., Ghosh A., Ojha D. K. *et al.* 2020, *MNRAS*, 498, 2309
- Skrutskie M. F., Cutri R. M., Stiening R. *et al.* 2006, *AJ*, 131, 1163
- Stetson P. B. 1987, *PASP*, 99, 191
- Stetson P. B. 1992, in *Astronomical Society of the Pacific Conference Series*, Vol. 25, *Astronomical Data Analysis Software and Systems I*, eds Worrall D. M., Biemesderfer C., Barnes J., p. 297
- Turbide L., Moffat A. F. J. 1993, *AJ*, 105, 1831
- Yadav R. K. S., Sariya D. P., Sagar R. 2013, *MNRAS*, 430, 3350
- Yeh F.-C., Carraro G., Korchagin V. I., Pianta C., Ortolani S. 2020, *A&A*, 635, A125